CFD MODELLING OF LARGE-SCALE LH2 SPILLS IN OPEN ENVIRONMENT

Venetsanos, A.G. [1], Bartzis, J.G. [2]
[1] Environmental Research Laboratory, National Center for Scientific Research Demokritos, Aghia Paraskevi, Attikis, 15310, Greece, e-mail: venets@ipta.demokritos.gr
[2] University of West Macedonia, Department of Energy and Resources Management Engineering, Kozani, Greece

ABSTRACT

In earlier work the 3d time dependent fully compressible CFD code ADREA-HF was applied against large-scale LH2 release experiments in the vicinity of buildings. In the present contribution the ADREA-HF code is applied to simulate large-scale LH2 spill tests in open, unobstructed environment. A series of simulations were performed to investigate on the effects of the source model (jet or pool), the modelling of the earthen sides of the pond around the source and the inclusion of a contact ground heat transfer. The predicted hydrogen concentrations (by vol.) are compared against the experimental at the available sensor locations. In addition the predicted structure of the concentration field is compared against the experimental, which was originally derived from temperature measurements. Modelling the source as a two-phase jet pointing downwards, including the modelling of the earthen sides of the pond as a fence and the contact heat transfer to the ground gave the best agreement with respect to experimental behaviour.

NOMENCLATURE

Roman

c_p	Specific heat under constant pressure	(J kg^{-1} K^{-1})
P	Pressure	(Pa)
T	Temperature	(K)
d	Molecular diffusivity of hydrogen to air	(m^2 s^{-1})
g_i	Gravity acceleration in the i-direction	(m s^{-2})
k	Turbulent kinetic energy	(m^2 s^{-2})
q_1, q_2	Mass fraction of component 1, 2	(-)
t	Time	(s)
u_i	i component of velocity	(m s^{-1})
U	Horizontal velocity	(m s^{-1})
u_*	Friction velocity	(m s^{-1})
x_j	Cartesian j co-ordinate	(m)
z	Cartesian z co-ordinate	(m)
z_0	Hydrodynamic roughness length	(m)
Pr_t	Turbulent Prandtl number	(-)
Sc_t	Turbulent Schmidt number	(-)
H	Enthalpy	(J kg^{-1})
H_g	Ground heat flux	(J m^{-2} s^{-1})
V,L	Subscripts denoting vapour and liquid	(-)

Greek

ε	Turbulent energy dissipation rate	(m^2 s^{-3})
κ	von Karman constant (= 0.4)	(-)
μ, μ_t	Laminar and turbulent viscosity	(kg m^{-1} s^{-1})
ρ, ρ_i	Mixture density, i-component density	(kg m^{-3})

1. INTRODUCTION

Hazard evaluation related to hydrogen release from cryogenic hydrogen storage has been the subject of several experimental and theoretical/computational studies in the past.

Large scale liquefied hydrogen dispersion experiments, simulating pipeline ruptures, were first performed by A D. Little Inc.., Lockheed California Co and the US Federal Bureau of Mines to examine the atmospheric dispersion behaviour of hydrogen, as a consequence of its increasing application in space aviation [1]. The amount of LH2 released was 19 m^3. The pipeline spill rate was on the order of several hundreds of gal min^{-1}. (1 gal min^{-1} = 0.0631 lt s^{-1}) The dispersion tests confirmed the decelerated buoyant behaviour of vaporized, but still cold gas and its tendency of a horizontal spreading with strong concentration fluctuations.

More than twenty years later experiments with large-scale releases of liquefied hydrogen were performed by NASA [2, 3] at White Sands, New Mexico, with aim to investigate the generation and dispersion of flammable clouds, formed as a result of large, rapid spills of liquid hydrogen. These types of spills might occur as the result of the rupture of a large storage facility. The experiments consisted of ground spills of up to 5.7 m^3 of liquid hydrogen (≈ 402 kg), with spill durations of approximately 35 seconds. Instrumented towers located downwind of the spill site gathered data on the temperature, hydrogen concentration and turbulence levels. Preliminary results from these experiments indicate that, for rapid spills thermal and momentum-induced turbulence cause the cloud to disperse to safe concentration levels and become positively buoyant long before mixing due to normal atmospheric turbulence becomes a major factor. The measurements also showed that ground level cloud travel extended approximately 50-100m from the source.

Later on, large-scale LH2 spill tests adjacent to buildings were performed by BAM [4, 5], in the framework of the EQHHPP project [6], in cooperation with Batelle Ingenieurtevhnik GmbH and the Research Center Jülich [7]. The aim of the experiments was to investigate the cryogenic pool spreading and vaporization, the generation of a gas/air mixture cloud and its dispersion. A total of 280 kg of LH2 was released in six tests and approximately 47 kg on the average per test.

Recently, small scale LH2 leakage and dispersion experiments were performed in the framework of the WE-NET project, [8, 9]. Early phase and steady phase pool spreading and evaporation as well as the cloud evolution were measured during these tests. Film boiling was observed during the early phase and the spreading liquid was divided into small spherical droplets by the gaseous evaporating phase. These droplets spread in rolling. During the steady phase nucleate boiling was observed and the rolling spread phenomenon disappeared.

Additionally INERIS performed large-scale, cryogenic Helium spill experiments with aim to simulate the scenario of the rupture of a connecting pipe in a LH2 system [10]. In total 10 tests were performed under different conditions. Maximum flow rates of 1.5 and 2.1 kg s^{-1} were reported, during several tens of seconds. During the tests temperatures were measured with thermocouples installed on a vertical grid 50x130 m made with steel ropes and erected along the wind direction with the help of two cranes. Concentrations were reduced from temperature data, assuming adiabatic mixing of helium with air (i.e. ground heat transfer neglected).

As far as simulations are now concerned, The NASA tests were simulated using the CHAMPAGNE code in [11], by performing two-dimensional (in the symmetry plane) two-phase flow calculations. The two phase flow model applied consisted of three mass conservation equations (liquid hydrogen, gaseous hydrogen and gaseous nitrogen), two momentum equations one for liquid hydrogen and one for gaseous hydrogen plus nitrogen and two energy equations one for each phase as for momentum. The comparison to the experimentally observed concentration field at 21.33 seconds was satisfactory. Comparison against measured concentration time series was not reported.

The measured pool spreading during the NASA tests was simulated in [7] using the LAuV shallow layer code. The predicted pool spreading was found overestimated with respect to the experimental

data. The same code was applied in [7] to simulate the pool spreading observed in the BAM tests. Here the comparison to the experiment was satisfactory.

CFD pre-test calculations of the BAM tests were performed using the Batelle code BASSIM [12], to help in the design of the experiments. Hydrogen was assumed released in gaseous form only. No associated post-experimental code validation was reported. Post test CFD dispersion calculations were performed using the FLUENT code [13] and the ADREA-HF code [14]. Gaseous hydrogen release conditions were assumed in [13] and this choice was used to justify the qualitative disagreement between predictions and experiment. Two phase flow release conditions were assumed in [14], in which the direct comparison against the experimental concentration and temperature data showed acceptable agreement, given the related uncertainties.

Finally reference [9] includes further development and validation of the CHAMPAGNE code against the WE-NET experiments. During this work the evaporation model in the CHAMPAGNE code was modified to take into account the rolling spread phenomenon, observed during the aforementioned experiments.

In the present work focus is given on the NASA trial-6 experiment. This test has been previously selected by HYSAFE NoE [15], as a case for a standard benchmark exercise problem (SBEP). This work reports a sensitivity analysis performed using the ADREA-HF CFD code [16] for simulation of the NASA-6 test. The reported results show the effects of the source model, of the presence of the elevated pond sides around the source and the effect of the contact heat transfer between ground and nearby ambient air.

2. EXPERIMENTAL CONDITIONS

The experimental system is described in detail in [2, 3]. The source was composed of a 5.7 m^3 Dewar, followed by a 10.2 cm line, which extended from an access hatch in the top to a location close to the bottom of the Dewar, followed by the 15.2 cm internal diameter foam insulated horizontal spill line approximately 30 m long, which was curved at its end vertically towards the ground ending to a diffuser (to minimize the momentum associated with the LH2 jet impact). Prior to the spill test, Dewar and 30 m line were filled with LH2. To conduct a spill gaseous helium was used to pressurize the Dewar to as high as 690 kPa. The valve at the end of the spill line was opened and LH2 was expelled vertically towards the ground. A 1.2 x 1.2 m steel plate 1.27 cm thick was located directly under the line exit to prevent earth erosion. The spill line dumped the LH2 into a 9.1 m diameter spill pond, which was constructed of earthen sides approximately 60 cm high with compacted sand as a bottom.

Meteorological conditions for test 6 were 2.2 m s^{-1} wind speed at 10m height, 15 ºC ambient temperature and 29% relative humidity.

Nine 19.5 m towers were deployed downwind of the spill pond. Concentration data from cloud sampling bottles were reported in [2] for tower 2, 1m elevation, tower 5, 1 and 9.4 m elevation and tower 7, 9.4 m elevation. Towers 2 and 5 were located on the “symmetry” plane 9.1 and 18.3 m distance from the centre of the spill pond respectively. Tower 7 was at 33.8 m from the centre of spill pond along the “symmetry” plane and 12.9 m laterally shifted. It must be noted here that lack of symmetry was recorded during the experiments, due to wind meandering, a fact which is also mentioned below when presenting the model predictions for tower 7.

Hydrogen concentrations deduced from temperature thermocouples readings (under the assumption of adiabatic hydrogen-air mixing conditions) were also reported in [2] for tower 2, 1m elevation, tower 5 9.4 m elevation and tower 7, 9.4 m elevation. In general good agreement was reported between sampling bottle data temperature deduced data.

3. MATHEMATICAL FORMULATION

The mean flow was modelled using the three dimensional transient, fully compressible conservation equations for mixture mass, mixture momentum, mixture enthalpy and hydrogen mass fraction.

Mixture mass (continuity equation)

$$\frac{\partial \rho}{\partial t} + \frac{\partial \rho u_i}{\partial x_i} = 0 \tag{1}$$

Mixture momentum

$$\frac{\partial \rho u_i}{\partial t} + \frac{\partial \rho u_j u_i}{\partial x_j} = -\frac{\partial P}{\partial x_i} + \rho g_i + \frac{\partial}{\partial x_j}\left((\mu + \mu_t)\left(\frac{\partial u_i}{\partial x_j} + \frac{\partial u_j}{\partial x_i} \right) \right) \tag{2}$$

Hydrogen mass fraction (liquid plus vapour):

$$\frac{\partial \rho q_1}{\partial t} + \frac{\partial \rho u_j q_1}{\partial x_j} = \frac{\partial}{\partial x_j}\left(\left(\rho d + \frac{\mu_t}{Sc_t} \right) \frac{\partial q_1}{\partial x_j} \right) \tag{3}$$

Mixture enthalpy

$$\frac{\partial \rho H}{\partial t} + \frac{\partial \rho u_j H}{\partial x_j} = \frac{\partial}{\partial x_j}\left(\frac{\mu_t}{\mathrm{Pr}_t} \frac{\partial H}{\partial x_j} \right) + \frac{dP}{dt} + \frac{\partial}{\partial x_j}\left(\lambda \frac{\partial \mathrm{T}}{\partial x_j} + \rho d H_i \frac{\partial q_i}{\partial x_j} \right) \tag{4}$$

In the above equations the mixture density is related to component densities (1V for hydrogen vapor, 1L for hydrogen liquid and 2 for air) and mass fractions through:

$$\frac{1}{\rho} = \frac{q_{1V}}{\rho_{1V}} + \frac{q_{1L}}{\rho_{1L}} + \frac{q_2}{\rho_2}; \quad 1 = q_1 + q_2; \quad q_1 = q_{1V} + q_{1L} \tag{5}$$

Turbulence was modelled using the standard k-ε model [17], in which buoyancy effects were included. In the ε-equation the coefficient multiplying the buoyancy production term was taken equal to the coefficient multiplying the mechanical production term. A value of 0.72 was assumed for the turbulent Schmidt and Prandtl numbers.

Evaporation was modelled using the equilibrium phase change model [18]. In this model it is assumed that the liquid phase of component-1 instantaneously evaporates, when the component-1 mass-fraction falls below its saturation value in the mixture (the reverse condition is taken as criterion for onset of condensation). The saturation mass fraction at given temperature and pressure is calculated using Raoult's law. The amount of component-1 in liquid phase is calculated from the requirement that a saturation state always exists in the gaseous region:

Ground heat transfer was modelled by solving a transient one dimensional energy (temperature) equation inside the ground.

4. MODELLING STRATEGY

The calculations were performed assuming symmetry plane at y = 0. The domain dimensions were 175x80x68 m in the x, y, z directions respectively. The source centre was at horizontal coordinates (25.65, 0.0), see also below. In the horizontal the minimum cell size was 0.6 m close to the source and the maximum was nearly 10 m close to the domain boundaries. In the vertical direction the minimum cell size was 0.2 m near the ground and source and the maximum cell size was about 9 m near the top

domain boundary. In general the grid expansion factor was below 1.2. The total number of computational cells was 39600.

Test-6 release data used in the present work were 5.11 m^3 LH2 released in 38 s, as in [3] (slightly different values were reported in [2]). The corresponding mass flow rate is 9.5 kg s^{-1}, assuming LH2 density = 70.8 kg m^{-3}.

The source was modelled in two different ways, as a two-phase downwards pointing jet and as a pool, in order to assess the resulting effect on the subsequent dispersion.

The modelling of the source as a jet was done as following. A horizontal open area source of size 0.5x0.5 m^2 pointing downwards was placed in the first cell next to ground at coordinates (25.65, 0.0, 0.1). This surface represented the diffuser. Boundary conditions on this surface were vertical velocity -11.47 m s^{-1}, pressure 101325.0 Pa, temperature 20.4 K (boiling) and void fraction (vapour volume/total volume) 97%. These conditions give hydrogen liquid mass fraction (liquid mass/total mass) 65%, hydrogen density equal to 3.315 kg m^{-3} and hydrogen flow rate equal to 9.5 kg s^{-1}. The amount of LH2 flashed vaporized at the source due to expansion from 690 kPa was the same as in [7].

The modelling of the source as a pool was done as following. A horizontal open area source of radius 4.45 m pointing upwards was assumed in place of the ground, centred at point (25.65, 0.0, 0.0). Boundary conditions on this surface were vertical velocity 0.2535 m s^{-1}, pressure 101325.0 Pa, temperature 20.4 K (boiling) and void fraction 100%. These conditions give hydrogen density equal to 1.207 kg m^{-3} and hydrogen flow rate equal to 9.5 kg s^{-1}.

In both cases the steel plate was not modelled. The ground was modelled as sandy with 3 mm hydrodynamic roughness length.

The earthen sides of the pond were modelled as a fence of very small thickness following [19]. The fence was assumed with a height 0.6 m, radius 4.55m centred at point (25.65, 0.0).

The important effect of ground heat transfer was identified in [14]. Ground heat transfer here is modelled as follows. The temperature difference between the air at the level of the centre of the first computational cell (next to ground) and the adjacent air at the level of the roughness length is related to the ground heat flux through the following wall function:

$$H_g = \frac{\kappa \rho c_p u_*}{\mathrm{Pr} \ln(z/z_0)} \left(T_{z0} - T\right) \tag{6}$$

To account for the temperature difference between ground (z = 0) and adjacent air at the level of the roughness length a contact heat transfer coefficient is defined as follows:

$$H_g = \rho c_p h_C \left(T_g - T_{z0}\right) \tag{7}$$

In the present work, the contact heat transfer coefficient was evaluated, according to [20]:

$$h_C = 10.395 \kappa u_* \left(\frac{\rho u_* z_0}{\mu} \right)^{-0.45} \tag{8}$$

The friction velocity entering the above equations was calculated as function of the horizontal velocity at the centre of the first cell through the following standard wall function relation:

$$\frac{U}{u_*} = \frac{1}{\kappa} \ln\left(\frac{z}{z_0} \right) \tag{9}$$

Table 1 shows the cases modelled.

Table 1. The computational grid main characteristics

Case	Source type	Fence	Contact heat transfer
1	Jet	Yes	Yes
2	Jet	Yes	No
3	Jet	No	Yes
4	Pool	No	Yes
5	Pool	Yes	Yes

For cases 1, 2 and 5, i.e. with fence present, the calculations were performed in three steps. First step was the one dimensional (in the z-direction) calculation of the approaching boundary layer. Second step was the three dimensional steady state calculation of the flow over the fence. Third step was the transient hydrogen release. The results of the first step were used as initial conditions for the second step and the results of the second step were used as initial conditions for the third. For cases 3 and 4, i.e. without the fence, only the first and third steps were applied.

Finally, discretization of the differential equations has been performed with the control volume method, using the first order fully implicit scheme for time integration and the first order upwind scheme for discretization of the convective terms [21]. Finally an automatic time step selection mechanism was applied with 0.001 seconds initial time step and 0.25 seconds as maximum permitted time value.

5. RESULTS AND DISCUSSION

Figures 1 to 5 show the predicted contours of hydrogen concentration (by volume) on the symmetry plane at time 21 seconds after the start of release. The black dots represent the measurement sensors (sampling bottles) on masts 2, 5 and 8. The centre of the source is at X = 25.65. The fence in Cases 1, 2 and 5 is between X = 21.1 and 30.2. Figures 1-5 should be compared against Figures 7 and 8 of [2] at times 20.94 and 21.33 seconds respectively. In these figures the centre of the source is estimated to be at downwind distance approximately 4.55 m, while the fence between 0 and 9.1 m.

Figure 6 shows the predicted hydrogen concentration (by vol.) time series compared against the available experimental data, which were extracted from [2].

A first general observation to be made is that as expected in all the present predictions drastic changes in cloud composition around 21 seconds after start of release were not observed, in contrast to experiment. Such very drastic changes were possibly associated with lateral cloud movements recorded during the experiments, indicative of wind meandering. In the present simulations the wind direction was taken constant along the X axis.

An additional general observation is that in all cases simulated the predicted concentrations at tower 7, 9.4 m elevation were significantly underestimated with respect to the experimental. This can also be attributed to wind meandering.

Focus now is given on the effects of the source model. As can be seen from figures 1-3, modelling the source as a two-phase jet directed downwards results in the part of the cloud having concentrations above 40% being restricted close to the source, both in the X and Z directions, in accordance with the reported experimental behaviour [2]. In contrast when the source is modelled as a pool, see figures 4 and 5 the corresponding high concentration region extends at least up to 15 m elevation. As a result the predicted levels of concentration at tower 2, 1m and tower 5, 9.4 m for cases 4 and 5 were found higher than for cases 1-3.

As far as ground heat transfer is concerned, a comparison between figures 1 and 2 shows the big importance of the contact heat transfer mechanism. Without this extra thermal resistance the cloud

gets extensively heated and detaches from ground at very short distance from the source, in contrast to experimental evidence [2]. As soon as the ground detaches from ground the first sensors affected are those closest to the ground. As a result the concentration levels at towers 2 and 5 at 1m elevation are for case 2 lower than for case 1.

Another important factor besides the ones previously mentioned is the presence of the fence. The barrier effect of the fence is most clearly seen by comparing Figures 1 and 3. In figure 3 the part of the cloud with concentrations between 36 and 40% is located at least 10 m downstream from the corresponding part in Figure 1, in contrast to experimental behaviour. The absence of the fence results in the cloud being more attached to the ground. As a result predicted concentration levels on tower 5, 1m for case 3 are higher than when the fence is present (case 1) and predicted concentrations at 9.4 m on the same tower for case 3 are lower than for case 1. The above mentioned effect of the fence removal on the cloud attachment downstream the source is less intense when the source is modelled as a pool, as can be observed from figures 4 and 5 compared to 1 and 3. This can be attributed to the way the pool was modelled, i.e. having an initial vertical momentum.

From the above discussion and related figures it is suggested that Case 1 is the closest to the experimental behaviour. For this case the predicted concentration levels on tower 5, 9.4 m are underestimated and at 1 m overestimated suggesting that the predicted cloud is less lifted from ground than in the experiment. This suggests that probably a more intense heat flux from the ground would be required to obtain a better agreement with the experiment.

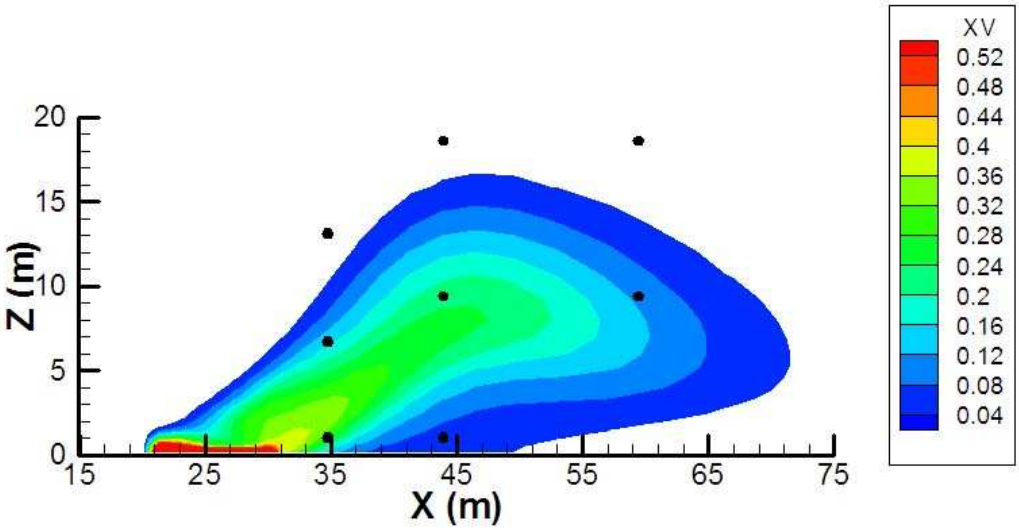

Figure 1. Predicted contours of hydrogen concentration (by vol.) on symmetry plane at t = 21 s (Case 1: Jet, with fence, with contact heat transfer)

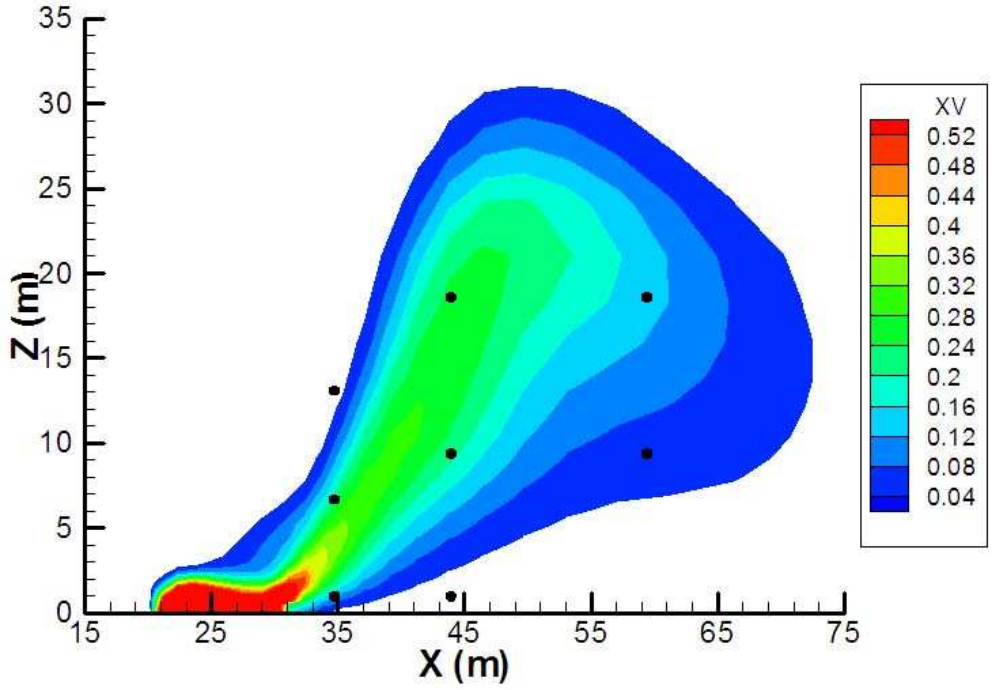

Figure 2. Predicted contours of hydrogen concentration (by vol.) on symmetry plane at t = 21 s (Case 2: Jet, with fence, without contact heat transfer)

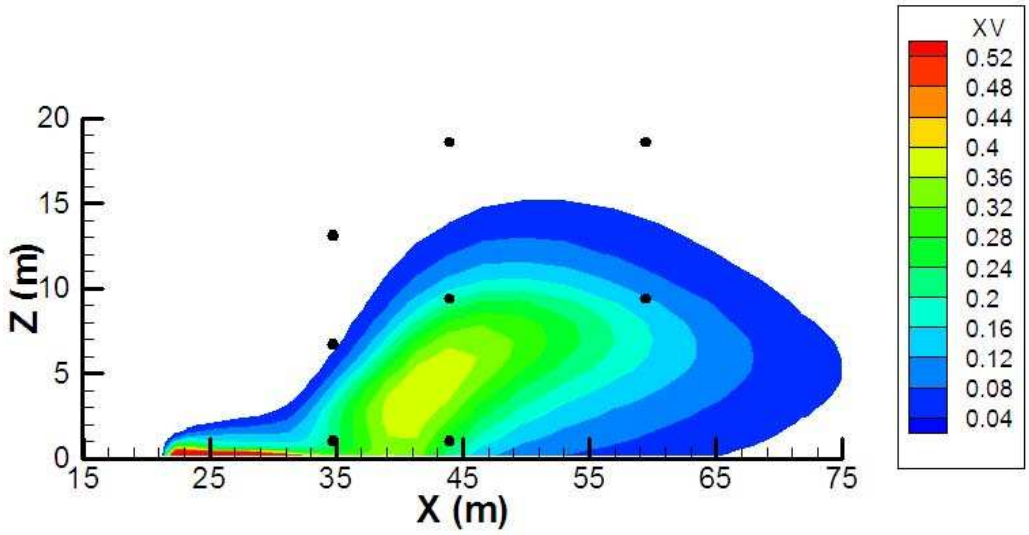

Figure 3. Predicted contours of hydrogen concentration (by vol.) on symmetry plane at t = 21 s (Case 3: Jet, without fence, with contact heat transfer)

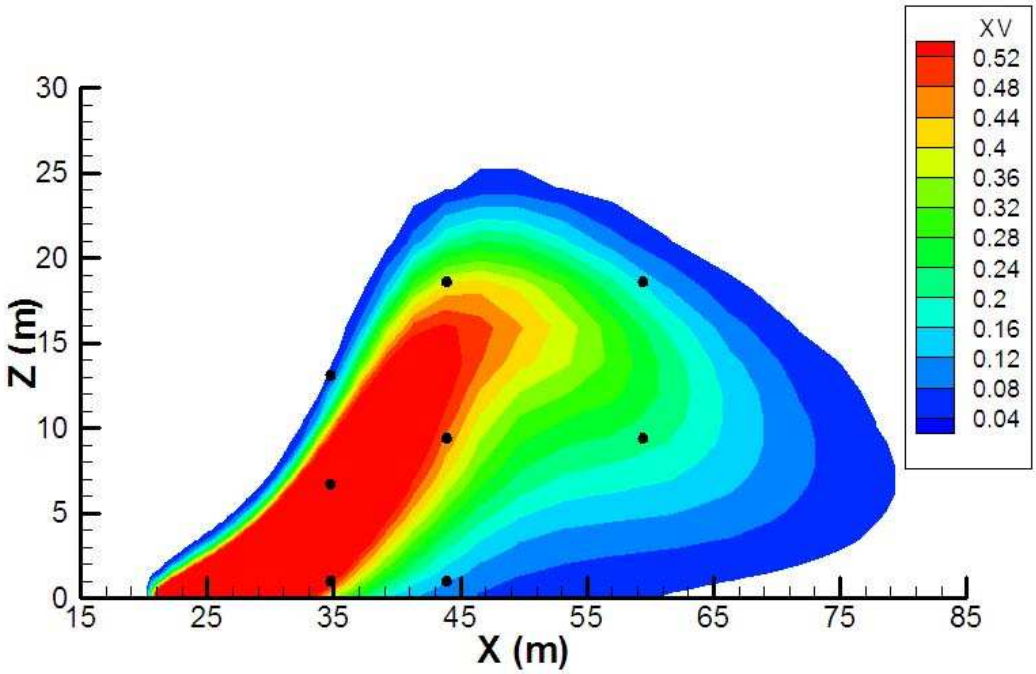

Figure 4. Predicted contours of hydrogen concentration (by vol.) on symmetry plane at t = 21 s (Case 4: Pool, without fence, with contact heat transfer)

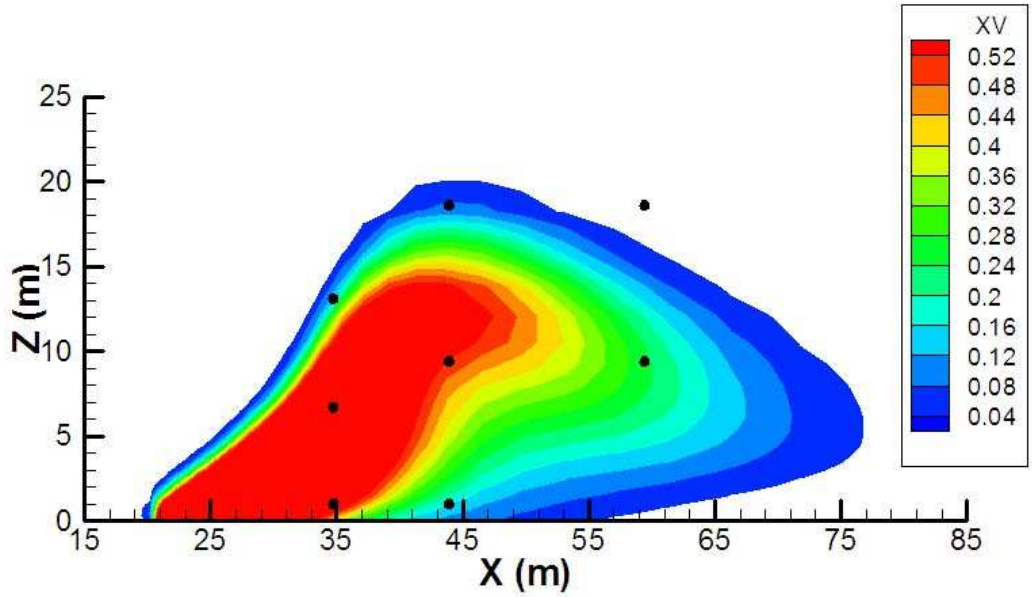

Figure 5. Predicted contours of hydrogen concentration (by vol.) on symmetry plane at t = 21 s (Case 5: Pool, with fence, with contact heat transfer)

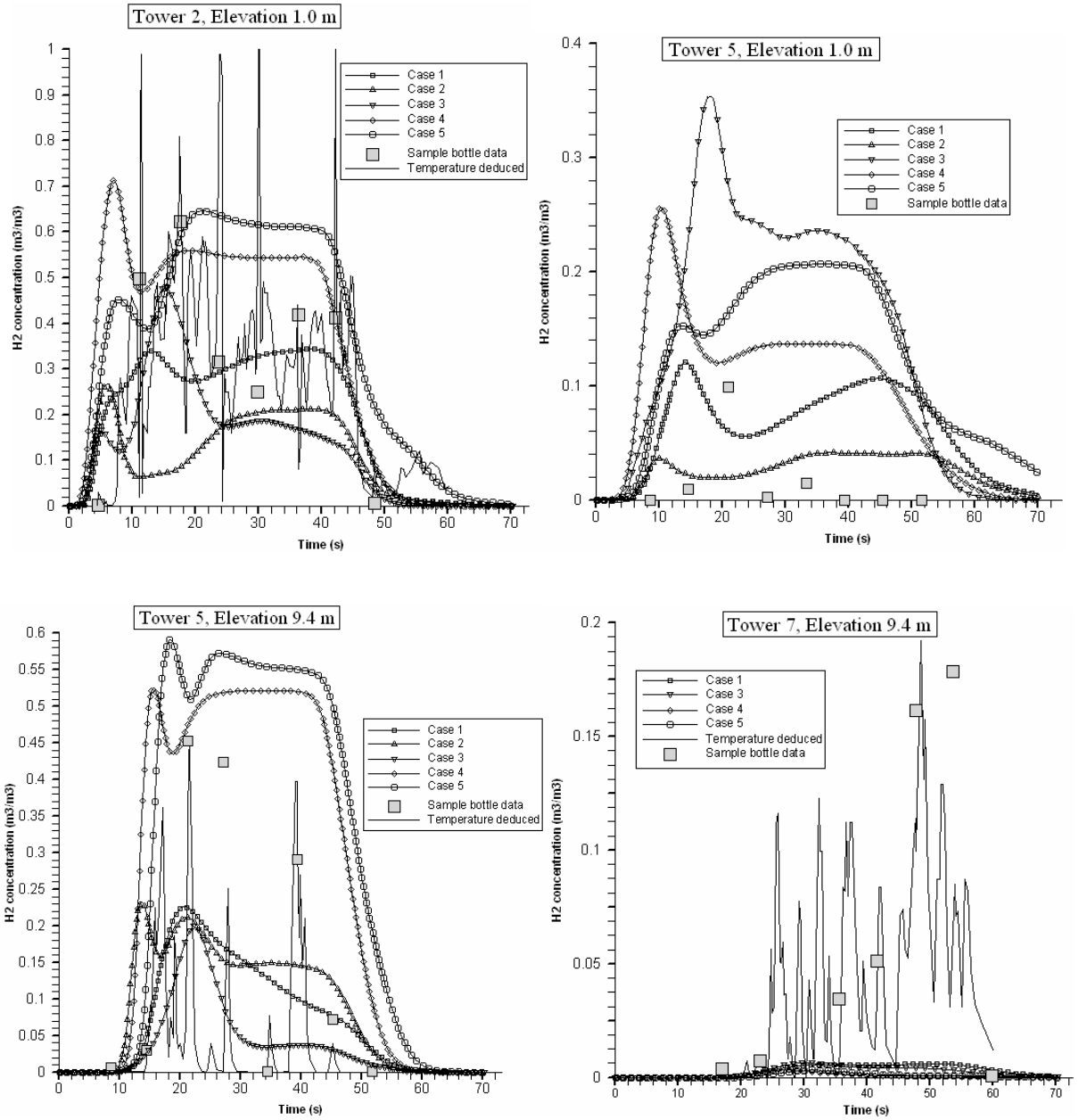

Figure 6. hydrogen concentration (by vol.) time series compared against the available experimental data, extracted from [2]. For cases see table 1.

6. CONCLUSIONS

The ADREA-HF CFD code was successfully applied to simulate the NASA trial-6 experiment. A series of CFD runs were performed to investigate on the effects of source model, fence presence and contact heat transfer. In all cases turbulence was modelled via the standard k-ε two-equation turbulence model, including buoyancy effects.

In all cases considered it was not able to reproduce neither the very sudden changes in cloud structure observed experimentally nor the high levels of concentrations measured at tower 7, located 33.8 m downwind and 12.9 m laterally from the source. This behaviour was attributed to wind meandering, observed during the experiments, but not modelled herein.

Entirely different cloud structures were obtained depending on the method the source was modeled. Modelling the source as a two-phase jet, pointing downwards resulted in predicted concentrations in much better agreement with the experiments. Modelling the source as a pool resulted in overestimation of concentration levels.

The earthen sides of the pond were modelled as a fence of infinitesimal thickness. The calculations showed that near ground concentration levels downstream the source increased when the fence was removed. This effect was more pronounced when the source was modelled as a jet.

Accounting for the temperature difference between ground and adjacent air at the level of the roughness length was found to be very important.

Using a two-phase jet pointing down, contact heat transfer and including the fence results were the closest to the experimental. Still, the predicted concentration levels on tower 5, 9.4 m are underestimated and at 1 m overestimated suggesting that the predicted cloud is less lifted from ground than in the experiment. This suggests that probably a more intense heat flux from the ground would be required to obtain a better agreement with the experiment.

7. ACKNOWLEDGEMENTS

The authors would like to thank the European Commission for funding of this work through the HYSAFE-NoE project under FP6.

8. REFERENCES

1. A. D. Little Inc., An Investigation of Hazards Associated with the Storage and Handling of Liquid Hydrogen, Final Report, Contract No AF-18 (600)-1687 (AD-324/94), 1960.
2. Witcofski R.D. and Chirivella J.E., Experimental and analytical analyses of the mechanisms governing the dispersion of flammable clouds formed by liquid hydrogen spills, *Int. J. Hydrogen Energy*, **9**, No. 5, 1984, pp. 425-435.
3. Chirivella J.E., Witcofski R.D., Experimental Results from Fast 1500 Gallon LH2 spills, Am. Inst. Chem. Eng. Symp. Ser. 82, No. 251, 1986.
4. Marinescu-Pasoi L., Sturm, B., Messung der Ausbreitung einer Wasserstoff- und Propangaswolke in bebautem Gelände and Gasspezifische Ausbreitungsversuche, Battelle Ingenieurtechnik GmbH, Reports R-68.202 and R-68.264, 1994.
5. Schmidtchen U., Marinescu-Pasoi L., Verfondern K., Nickel V., Sturm B., Dienhart B., Simulation of accidental spills of cryogenic hydrogen in a residential area, Cryogenics 34, 1994, pp. 401-404 (ICEC 15 Supplement).
6. Gretz J., Drolet B., Kluyskens D., Sandmann F., Ullmann O., Phase II and Phase III,0 of the 100 MW Euro-Quebec Hydro-Hydrogen Pilot Project EQHHPP, Proc. 9th World Hydrogen Energy Conference, published by MCI, Paris, 1992, Vol. 3, pp. 1821.
7. Verfondern K. and Dienhart B., Experimental and theoretical investigation of liquid hydrogen pool spreading and vaporization, *Int. J. Hydrogen Energy*, **22**, No. 7, 1997, pp. 649-660.
8. Hijikata T., Research and development of international clean energy network using hydrogen energy (WE-NET), *Int J. Hydrogen Energy*, **27**, 2002, pp. 115-129.
9. Chitose K., Takeno K., Yamada Y., Hayashi K. and Hishida M., Activities on Hydrogen Safety For the WE-NET Project – Experiment and Simulation of the Hydrogen Dispersion, Proceedings of WHEC-14, Toronto 2002.
10. Proust C., Chelhaoui S., Joly C., Process of the formation and explosion of hydrogen-air clouds following and extensive spillage of liquid hydrogen, Poster presented at the NHA conference, Washington, US, 2001.
11. Chitose K., Ogawa Y., Morii T., Analysis of a large scale liquid hydrogen spill experiment using the multi-phase hydrodynamics analysis code CHAMPAGNE, (WHEC-11, Stuttgart, FRG, 1996),

(editor T.N. Veziroglu et al. at Hydrogen Energy Progress XI, International Association for Hydrogen Energy, 1996, pp. 2203-2211).
12. Rastogi A.K., Marinescu-Pasoi L., Numerical simulation of hydrogen dispersion in residential areas, 10th World Hydrogen Energy Conference, Cocoa Beach, US, 1994, pp. 245-254.
13. Schmidt D., Krause U., Schmidtchen U., Numerical simulation of hydrogen gas releases between buildings, *International Journal of Hydrogen Energy,* **24**, 1999, pp. 479-488.
14. Statharas J.C., Venetsanos A.G., Bartzis J.G., Würtz J., Schmidtchen U., Analysis of data from spilling experiments performed with liquid hydrogen, *Journal of Hazardous Materials,* A77 (1-3), 2000, pp. 57-75.
15. HYSAFE Network of Excellence, www.hysafe.org, EC-FP6 Contract No SES-6-CT-2004-502630.
16. Bartzis, J. G., ADREA-HF: A three dimensional finite volume code for vapour cloud dispersion in complex terrain, EUR report 13580 EN, 1991
17. Launder B. E. and Spalding, D. B., The numerical computation of turbulent flow, *Computer Methods in Applied Mechanics and Engineering*, **3**, Issue 2, 1974, pp. 269-289.
18. Venetsanos A.G., Bartzis J.G., Würtz J., Papailiou D.D., DISPLAY-2: A two-dimensional shallow layer model for dense gas dispersion including complex features, *Journal of Hazardous Materials*, A99, 2003, pp. 111-144.
19. Andronopoulos S., Bartzis J.G., Würtz J., Asimakopoulos D., Modelling the effects of obstacles on the dispersion of denser than air gases, *Journal of Hazardous Materials*, **37**, 1994, pp. 327-352.
20. Zilitinkevich S.S., Dynamics of the Atmospheric Boundary Layer, Leningrad, Gidrometeor., 1970, pp. 291.
21. Patankar, S. V., Numerical heat transfer and fluid flow, 1980, Hemisphere Publishing Corporation.